Post-Impact Residual Strength and Resilience of Sandwich Panels with Natural Fiber Composite Faces

Dillon Betts[1], Pedram Sadeghian[2], and Amir Fam[3]

ABSTRACT: In this paper, the post-impact residual flexural behavior of sandwich panels with flax fiber-reinforced polymer (FFRP) faces and polyisocyanurate (PIR) foam cores is investigated experimentally. The faces were manufactured using a wet lay-up procedure with a balanced bidirectional 2x2 twill flax fiber fabric and a bio-based epoxy with a bio-content of 30%. Each specimen was 1200 mm long x 75 mm wide x 80 mm thick. The main parameters in the study were the face thickness (one, two or three FFRP layers, representing core-to-skin thickness ratios of approximately 54, 28 and 20) and core density (32, 64 or 96 kg/m^3); a total of nine combinations. In this study, 27 specimens (three specimens for each combination) were tested under impact loads and the surviving specimens were tested under monotonic three-point bending. Each of the three identical specimens was tested under different impact condition, namely 100%, 75% and 50% of the energy resistance of an intact specimen, with the last two impacted 50 times. The results of the post-impact residual flexural tests were compared to three-point bending tests of intact specimens. The beams demonstrated remarkable resilience in that the impact events did not have a negative effect on their flexural strength or stiffness. In fact, those tested at higher energy levels exhibited a slight increase in strength after impacts. This shows their suitability for use in infrastructure applications such as building cladding panels, flooring and roofing as they retain their strength and stiffness even after

[1] PhD Candidate, Department of Civil and Resource Engineering, Dalhousie University, 5268 DaCosta Row, Halifax, NS B3H 4R2, Canada. Email: dillonbetts@dal.ca (corresponding author)
[2] Associate Professor and Canada Research Chair in Sustainable Infrastructure, Department of Civil and Resource Engineering, Dalhousie University, 5268 DaCosta Row, Halifax, NS, B3H 4R2, Canada. Email: pedram.sadeghian@dal.ca
[3] Donald and Sarah Munro Chair Professor in Engineering and Applied Science and Associate Dean (Research), Department of Civil Engineering, Queen's University, Kingston, ON, K7L 3N6, Canada. Email: amir.fam@queensu.ca

multiple impacts.

DOI: 10.1016/j.jobe.2021.102184

KEYWORDS: Sandwich Structures, Natural Fibers, Flax, Sustainable Infrastructure, Impact, Residual Behaviour

INTRODUCTION

With the growing understanding of the effect of human activity on the environment, it is important to consider ways to reduce the environmental footprint caused by civil infrastructure including buildings. One way to improve the sustainability of building practices is the use of systems that provide dual benefits, such as sandwich panels. These are lightweight systems that are comprised of strong and stiff faces and a lightweight core, such as foam, that separates the faces and increases the moment of inertia. When used for building cladding applications, sandwich panels can provide both lateral force resistance and insulation. The environmental sustainability of sandwich panels can be further improved through the use bio-based materials. Sandwich panel faces are often constructed of metals or synthetic fiber-reinforced polymers (FRPs), such as glass FRPs. Because these materials are much stronger than the weaker core material, sandwich panel failure often occurs in the core and therefore the strength of the face material is underutilized [1,2]. This leaves an opportunity to replace these synthetic face materials with bio-based materials, such as FRPs made with natural fibers, such as flax and bio-based polymers. Flax fibers are relatively strong and stiff compared with other natural fibers [3] and have less embodied energy than glass or carbon fibers [4]. Sandwich panels with flax FRP (FFRP) faces and foam cores are a more sustainable alternative for construction applications, such as cladding for building envelopes. Before they can be implemented in the industry, it is necessary to have an in-depth understanding of the behaviour of sandwich panels with FFRP faces

under various loading conditions, such as shear and flexural loading, impact loading and post-impact flexural loading.

Sandwich panels with synthetic FRP faces have been studied extensively under flexural loads [5–12] and recently, some researchers have focused on the shear and flexural behavior of sandwich panels with natural FFRP faces and foam cores [2,13–16]. Due to their light weight and insulative properties, sandwich panels are often used for building cladding. During windstorms, building envelopes can be impacted by flying debris and therefore it is important to understand their impact behavior. Therefore, the low velocity impact behavior of sandwich structures with synthetic faces has been well documented in the literature [17–23]. Recent studies have also looked at the impact behavior of sandwich panels with FFRP faces and foam cores [24–26]. Other authors have studied the high strain rate behavior of FFRPs and other natural FRPs [27,28]. Kim et al. [28] performed high rate compression tests on hemp, glass and hybrid composites with different matrices. They found that between strain rates of 600 strain/s to 1500 strain/s the hemp-thermoset composites exhibited maximum stresses similar to that of glass composites. However, after 1500 strain/s, there was no significant increase in strength with strain rate and it was concluded that strain hardening was muted above this strain rate. Hu et al. [27] examined the high strain rate compressive behavior of FFRPs made with woven flax fabrics loaded in-plane and out-of-plane. They determined that FFRPs exhibited higher strength in both the in-plane and out-of-plane directions under high strain rate loads.

Building envelopes may be impacted multiple times throughout their lifespan, and therefore an understanding of their post-impact residual strength and resiliency is necessary. Numerous studies have focused on the compression after impact (CAI) test to determine the post-impact residual strength of impacted sandwich panels [29–31]. However, sandwich panels in building cladding systems are typically required to resist flexural loads and therefore it is appropriate to test their flexural

behavior after impact. Tests to determine the residual flexural strength of sandwich panels with GFRP faces [32] and CFRP faces [33–35] have been performed. Baran and Weijermars (2020) looked at the post-impact flexural behavior of sandwich panels with GFRP faces and multiple different core types, including: balsa wood, styrene acrylonitrile foam and polyethylene terephthalate foam. They observed a reduction in both strength and stiffness of impacted specimens compared with intact specimens due to the impact event. He et al. (2018) studied sandwich panels with CFRP faces and corrugated aluminum cores. After impacting specimens at various energy levels, they tested them under three-point bending. The authors noted that there was a reduction in specimen strength due to all levels of impact and they concluded that the main cause of the decrease in strength was local buckling of the aluminum core under the area of the impact.

There is currently a gap in the literature with respect to the post-impact residual strength and resilience of sandwich panels with FFRP faces. The aim of this paper is to fill this gap by providing experimental data on the post-impact flexural behavior of sandwich panels with FFRP faces and foam cores. Furthermore, the resiliency of these panels is tested through post-impact flexural testing of specimens that have been impacted at one energy level multiple times.

EXPERIMENTAL PROGRAM

As a part of this study, sandwich beams with FFRP faces and PIR foam cores were impacted with a drop weight and subsequently tested under three-point bending to determine the residual flexural behaviour. In this section of the paper, the test matrix will be presented as well as the specimen fabrication and test set-up and procedure.

Test Matrix

A total of 27 sandwich beams which were 1200 mm long, 75 mm wide and 80 mm thick, were tested. The main test parameters were the face thickness, foam core density and impact energy level. Three

face thicknesses were examined: one layer, two layers and three layers of FFRP per face which were measured to be 1.41 ± 0.16 mm, 2.70 ± 0.15 and 3.90± 0.17 mm thick, respectively. The core-to-thickness ratios of the one-layer, two-layer and three-layer beam specimens were 54, 28, and 20 respectively. Foam cores with three densities were examined: 32 kg/m^3, 64 kg/m^3 and 96 kg/m^3. The effects of three impact energy levels were investigated: 100% 75% and 50% failure energy.

The test matrix is presented in Table 1. The following naming convention was used: XFL-YC-RZ, where X is the number of FFRP layers in each face, FL represents "Flax Layers", Y is the core density in kg/m^3, C represents "Core", R represents "Residual", and Z is the energy level of the impact tests as a percentage of the energy resisted by intact specimens. For example, a specimen with two layers of FFRP on each face and a core density of 96 kg/m^3 impacted at 75% the energy resisted by an intact specimen would be labelled 2FL-C96-R75.

In this study, there were nine sets of three specimens with the same face thickness and core density. The first set (group R100) were each impacted once at 100% the failure energy resisted by similar specimens tested under ramped impact loading [36]. It was expected that this impact would cause failure in the specimens, as it had in previous tests. However, eight of the nine specimens survived the impact event. As the previously tested specimens [36] were impacted multiple times before failure, it is assumed that the cumulative energy absorption affected the ultimate impact capacity of the panels predicted by these tests. Therefore, the impact energy for the remaining tests (groups R50 and R75), was determined based on the energy to cause failure in quasi-static tests of similar specimens [13]. The R100 specimens were subsequently tested under three-point bending to determine the post-impact residual flexural behavior. Through these tests, as will be discussed later, it was determined that the one impact at 100% energy did not significantly affect the behaviour of the beams. The second set (group R75) were each impacted 50 times at 75% of the energy resisted by

intact specimens. Only three of these specimens survived the impact tests. It should be noted that the first two specimens tested in the R75 group (1FL-C32-R75 and 2FL-C32-R75) were tested at 90% failure energy. The intent was to test the entire group at 90% energy, but when these two specimens failed after a low number of impacts, the impact level was reduced in order to avoid all specimens failing before residual tests could be performed. The third set of specimens (group R50) were each impacted 50 times at 50% of the energy resisted by intact specimens. All but one specimen survived the impacts. The R75 and R50 specimens were then tested under three-point bending to determine their post-impact residual behavior and resiliency to multiple impacts.

It should be noted that the R100 impact energy was set to the maximum energy resisted by impact test specimens from a previous study [26] whereas the R75 and R50 impact levels were determined by finding the energy to cause failure in specimens tested under quasi-static bending in a previous study [13]. As discussed above, this was decided after testing the R100 specimens and determining that the failure energy from the impact test specimens was potentially low due to cumulative energy absorbed from multiple impacts before failure. Also note that the R100 specimens were 150 mm wide, but in order to directly compare the results of the tests, all test data presented in this paper was normalised to a beam width of 75 mm. One notable drawback of the test matrix is that only one specimen was tested at each energy level and therefore it should be noted that the conclusions of this study are based on single tests. However, as nine different specimen types were tested under each loading condition, general conclusions of the resiliency of the FFRP-foam sandwich beams can be made with confidence.

Materials

All sandwich panels were constructed of FFRP faces and PIR foam cores. Foams with three different nominal densities were used, namely 32, 64 and 96 kg/m^3 (ELFOAM P200, P400 and P600, Elliott

Company, Indianapolis, IN, US). The FFRP used was fabricated using a 2x2 twill flax fabric (Biotex Flax, Composites Evolution, Chesterfield, UK) with an areal density of 410 g/m^2 and a bio-based epoxy resin with an approximate bio-content of 30% after mixing (ONE Epoxy, Entropy Resins, Hayward, CA, US). Betts et al [13] tested these FFRPs to determine their tensile and compressive behavior. The average (± standard deviation) initial tensile modulus, strength and ultimate strain of the FFRP faces were found to be 7.51 ± 0.69 GPa, 45.4 ± 1.8 MPa and 0.0083 ± 0.0009 mm/mm, respectively. The average (± standard deviation) initial compressive modulus, strength and corresponding strain were found to be 6.73 ± 1.59 GPa, 86.4 ± 2.2 MPa and 0.0327 ± 0.0010 mm/mm, respectively. Previous studies have also noted that FFRPs and other natural fibre composites exhibit a nonlinear behavior [37–40].

Specimen Fabrication

The specimen fabrication procedure is presented in Figure 1. First, the foams were cut down to a size of 600 mm by 1200 mm. A 600 mm wide sandwich panel was fabricated using this foam section that was later cut into individual beams for testing under quasi-static flexural loads [13], ramped impact loads [36], and post-impact residual loads in the current study.

To fabricate the sandwich panel, the flax fabric was cut to the correct width using scissors as shown in Figure 1a. The surface of the foam was cleaned of all dust and debris using a brush as shown in Figure 1b. Once, the fabric was prepared and the surface of the foam was clean, the bio-based epoxy was mixed and applied to the surface of the foam as shown in Figure 1c. The first layer of flax fabric was then applied to the wetted foam surface with the warp direction of the fabric parallel to the longitudinal direction of the foam. Epoxy was then placed and spread across the fabric as shown in Figures 1d and 1e. Depending on the desired FFRP thickness, more flax layers were placed in the same manner. When the correct amount of flax fabric layers had been added (one, two or three),

parchment paper was placed on the surface and an aluminum roller was used to remove excess resin and air as shown in Figure 1g. A weighted board was then placed on the surface of the panel as shown in Figure 1h and the face was allowed to cure for a minimum of seven days before cutting. This entire procedure was repeated for the opposite face of each panel. When both faces were cured, each panel was cut into the individual specimens using a band saw. As noted previously, the R100 specimens were cut to width of 150 mm, while the R75 and R50 specimens were cut to a width of 75 mm.

Test Setup and Instrumentation

In this study, each beam went through two phases of testing: impact tests and post-impact quasi-static flexural testing. The R100 specimens were each impacted once before post-impact tests, while the R50 and R75 specimens were each impact 50 times before post-impact testing. In this section, the set-up of each testing phase will be presented and discussed.

Impact Tests

To impact the specimens, a drop weight frame based on ASTM D7136 [41] was used. A photo of the test set-up with a 75 mm wide specimen in place is shown in Figure 2. A 10.4 kg drop weight with a 150 mm wide impact surface impacted the specimens at midspan. The 150 mm wide impact surface was chosen to mitigate premature a local failure mechanism as the intent of the tests was to observe the global response of these sandwich beams and to simulate the behavior due to the impact of large wind-borne debris. Additionally, the 150 mm impactor matched the loading surface used in the quasi-static tests by Betts et al [13] allowing for direct comparison of the tests. The impact surface was made using a piece of a steel hollow structural section (HSS) with rounded edges to reduce any stress concentrations occurring at the edge of the loading area. The length of the impact surface was long enough such that the full width of each specimen was impacted. At both ends a specimen rebound restraint was added to ensure the specimens did not bounce after being impacted. Each support was

made using a steel roller, one end was welded to the frame to simulate a pin support while the other end was placed to simulate a roller support. Each specimen was impacted either one time (R100 specimens), 50 times (R50 and R75 specimens) or until failure.

Post-Impact Flexural Tests

The post-impact flexural tests were performed based on ASTM D790 [42] with minor modifications, such as the width and shape of the loading area. A schematic and photos of the test set-up are presented in Figure 3. It is important to note that the sandwich beams were tested in the same configuration as in the impact tests; the top face during the impact tests was also the top face during the post-impact flexural tests. The test frame used was bolted to a concrete strong floor. At each end the specimens were supported on roller-type supports resting on steel pedestals which were placed on the concrete strong floor. A concentrated load was applied to the beams through a 150 mm by 150 mm steel HSS section with a length long enough to ensure that each specimen was loaded across its full width. The HSS had a mass of 8.1 kg which was included in the data processing. A hydraulic actuator with a load cell attached applied displacement to the HSS a rate of approximately 15 to 20 mm per minute. For the 150 mm wide specimens, a 250 kN load cell was used. However, a 45 kN load cell was used to test the 75 mm specimens to improve the accuracy at the lower load levels. A string potentiometer was used to measure the deflection at midspan and strain gauges with 6 mm gauge lengths were used to measure the strain in each face at midspan. All data was sampled at a rate of 10 Hz.

RESULTS AND DISCUSSIONS

In this section of the paper, the results of the tests will be presented and discussed. Generally, the data processing was performed using a script written using the scientific package, Anaconda, for the programming language, Python. The results of the tests in terms of strength and stiffness are presented in Table 2 and Table 3, respectively.

Failure Modes

The failure modes of all specimens are presented in Figure 4. In order to compare the residual failure modes with the failure modes observed during static tests, photos of sandwich specimens tested as a part of another study by Betts et al [13] were presented. The only notable difference in failure mode between tests of similar specimens is the failure of 1FL-C64-R75. This specimen failed due to tensile rupture during the post-impact residual flexural tests whereas the intact static specimen failed due to crushing of the compression face. This can be explained by the fact that damage in the form of visible tensile cracks was observed on the bottom face of this specimen after the impact tests. Tensile cracks were also observed in the C96-R50 specimens, sample photos of which are presented in Figure 5. However, the static C96 specimens failed due to tensile rupture and therefore the failure modes of the C96 specimens were not affected. Interestingly, as shown in Table 2, the strength of 1FL-C96-R50 and 2FL-C96-R50 were reduced, however the load capacity of 1FL-C64-R75 was higher than its static counterpart by 19%. Further research is required to determine the cause of this increase in strength of the post-impact residual tests.

Impact Tests

Some specimens failed during the impact phase of the testing. The number of impacts before failure is presented in Table 1. One R100 specimen, 2FL-C96-R100, failed during the impact tests. The R100 impact energies were based on the energy resisted in a previous set of impact specimens that were tested by [26]. Because these specimens were tested at drop height increments of 100 mm, it is possible that this specimen was close to energy that caused failure in the previous specimen.

For the R75 specimens, only the C64 type specimens survived the impact tests. It is hypothesized that this is based on the respective resiliency of the PIR foams and the FFRP faces. The C32-R75 specimens all failed from a core type failure, which indicates that the resiliency of the sandwich beams

was limited by the 32 kg/m^3 foam. This is supported by the fact that the C64 specimens with similar face thicknesses were able to withstand higher impact energies. Similarly, it is hypothesized that as the C96-R75 specimens failed due to tensile rupture, that the resiliency of these specimens was limited by the resiliency of the FFRP faces. These hypotheses indicate that the C64-R75 specimens were at a balance point.

Of the R50 specimens, only 3FL-C32-R50 failed during the impacts. It is assumed that this is again due to the lack of resiliency of the 32 kg/m^3 foam. As specimens 1FL-C32-R50 and 2FL-C32-R50 were tested at lower energies, the capacity of the foam at the lower impact energies was sufficient enough to survive the impacts. Additionally, because 3FL-C32-R50 was tested at a lower energy than the corresponding R75 specimen, it was able to withstand more impacts before failure. As shown in Table 1, 3FL-C32-R50 failed after 24 impacts, whereas 3FL-C32-R75 failed after only 3 impacts.

Residual Behavior After Impact

Load-Deflection Behavior

The load-deflection curves of all specimens are presented in Figure 6. Additionally, the load capacity and initial stiffness of each specimen tested under residual bending are presented in Table 2 and Table 3, respectively. Initial stiffness was taken as the initial slope of the load-deflection curves presented in Figure 6. This initial stiffness is based on both the shear and flexural deflections which are both prevalent in sandwich beams. Therefore, it is suitable metric to investigate the effect of impact on the sandwich beams tested in this study. Figure 6 shows that the post-impact behavior is similar to the behavior of the intact specimens. Table 2 shows that there was generally no reduction of strength in the post-impact bending tests. In fact, some specimens showed an increase in strength in post-impact tests. To examine this behaviour further, paired t-tests with a confidence levels of 95% were performed using Microsoft Excel to compare each set of specimens to their intact static specimen

counterparts. The results of the t-tests showed that there was no significant difference between the intact static load capacities and the load capacities of the R50 specimens. However, the t-tests indicated that, the means of the load capacities of the R75 and R100 specimen sets were statistically significantly higher than their intact static counterparts. This increase in strength is not yet well understood and requires further research. One hypothesis for this increase in strength is the potential continued curing of the faces between the quasit-static tests performed by Betts et al [13] and the post-impact flexural tests presented in the current study. The tests performed as a part of this study were performed over a year after the initial quasi-static tests. Therefore, there is the potential that the epoxy used for the faces continued to gain strength in the period between the tests. This potential increase in FFRP strength due to curing time should be investigated in future studies by fabricated FFRP tension coupons and testing them after set amounts of curing time. Paired t-tests with confidence levels of 95% were also performed to examine the post-impact beam stiffnesses. The t-tests showed that there was no statistical difference between the stiffnesses of the intact and impacted specimens.

In order to directly compare the results of all the tests and to show that there was no effect on residual behavior due to the impact events, the residual load capacity and stiffness of all specimens were plotted against the impact load energy, face thickness and core density in Figure 7. Figure 7a shows the effect of the energy level (regardless of number of impacts) on the residual load capacity and stiffness. This figure confirms that the energy level of the impacts did not have a significant effect on the residual load capacity of the beams. Figure 7b and Figure 7c show effects of core density and face thickness on the residual capacity and stiffness. These plots show that both the residual capacity and stiffness were significantly affected by both the core density and face thickness.

Load-Strain Behavior

The load-strain curves are presented in Figure 8. Based on the plots, there is some phenomenon affecting the strain in the top faces of the R50 and R75 specimens. The top face strain of these specimens is softer than the intact specimens at low load levels. It is hypothesized that this softening was caused by the development of microcracks in the matrix of the compression face during the impact events. Though there were no visible cracks observed on the compression faces, it is possible that there were cracks there that could not be seen with the naked eye. Figure 9 presents a diagram on the potential development of these cracks in the compression face and the resulting softening of the post-impact load-strain behavior of the top face. It should be noted that previous studies on the bending after impact behavior of sandwich structures [32–35] focused on the load-deflection response and did not show the strains in the top and bottom faces. Therefore, this hypothesis has not been verified and this strain softening in the top face should be investigated further in future studies.

Each impact induced free vibration in the sandwich beams. During this free vibration the faces of the sandwich beams repeatedly changed between states of tension and compression until the beam returns to a state of rest. Therefore, it is possible for tensile cracks to have developed in the matrix of both faces during the impact events. When the sandwich beams were subsequently tested under three-point bending, the microcracks in the matrix of the top face would have to close before the full stiffness of the FFRP could be developed. This is not the case for the bottom tensile face, which is why this phenomenon was only observed on the top faces.

As shown in Figure 8, this load-strain softening was not observed in the R100 specimens. As it only affected the residual specimens that were impacted 50 times and not the R100 specimens, that were impacted once at a higher energy level, this indicates that this behavior was caused by the repeated impacts.

Moment-Curvature Behavior

The moment-curvature diagrams for all specimens are presented in Figure 10. Based on the diagrams, the initial flexural rigidity of the R50 and R75 specimens was significantly reduced after impacts. As the curvature was calculated based on the measured face strains, this softening of the moment-curvature diagrams is directly caused by compressive load-strain behavior discussed earlier. The moment-curvature plots also show that the ultimate curvature of the C32 type specimens is lower than both the C64 and C96. This is because of the weaker core foams that governed failure and is evidence for these specimens, the strength of the FFRP faces was underutilized. The plots also show that the FFRP faces of the C64 specimens were underutilized as well, but to a lesser degree.

CONCLUSIONS

In this paper, the results of post-impact flexural tests on sandwich beams with flax fiber-reinforced polymer faces and polyisocyanurate foam cores were presented. A total of 27 sandwich beams were tested as a part of this study. The main parameters of the tests were the face thickness (one, two or three layers of flax fabric), the core density (32 kg/m^3, 64 kg/m^3 or 96 kg/m^3), and the impact energy and quantity (50 impacts at 50% the energy resisted by an intact sandwich beam, 50 impacts at 75% energy or one impact at 100% energy). Based on the tests, the following conclusions were made:

- The FFRP-foam sandwich beams exhibited notable resiliency. The post-impact flexural tests showed that the impacts did not cause a reduction in strength or stiffness of the sandwich beams.
- For specimens impacted at higher impact energies (75% and 100% of the energy resisted by intact specimens), there was a statistically significant increase in specimen strength after the impact events. Further research is required to explain this phenomenon.

- The failure modes of the sandwich beams were relatively unaffected by the impact events. The only specimen that exhibited a significant change in failure mode was 1FL-C64-R75 which failed due to tensile rupture of the bottom face whereas the intact beam failed due to compression face crushing. This change in failure mode was caused by the development of tensile cracks during the impact testing procedure.
- Sandwich beams impacted 50 times exhibited a softening of the load-top face strain behavior and reduction in initial flexural rigidity during the post-impact flexural tests. This reduction was attributed to the hypothesized development of microcracks in the matrix of the top face. However, this has not been verified and should be investigated further in future studies.

ACKNOWLEDGEMENTS

The authors would like to thank Lauren MacDonnell, Yuchen Fu, Jesse Keane, Brian Kennedy and Jordan Maerz for their assistance in the lab. The authors would also like to acknowledge and thank NSERC, Queen's University, and Dalhousie University for their financial support.

DATA AVAILABILITY STATEMENT

Data associated with this study is available upon request.

REFERENCES

[1] Fam A, Sharaf T, Sadeghian P. Fiber element model of sandwich panels with soft cores and composite skins in bending considering large shear deformations and localized skin wrinkling. J Eng Mech 2016;142:1–14. doi:10.1061/(ASCE)EM.1943-7889.0001062.

[2] Sadeghian P, Hristozov D, Wroblewski L. Experimental and analytical behavior of sandwich composite beams: Comparison of natural and synthetic materials. J Sandw Struct Mater

2018;20:287–307. doi:10.1177/1099636216649891.

[3] Ramesh M, Palanikumar K, Reddy KH. Plant fibre based bio-composites : Sustainable and renewable green materials. Renew Sustain Energy Rev 2017;79:558–84. doi:10.1016/j.rser.2017.05.094.

[4] Cicala G, Cristaldi G, Recca G, Latteri A. Composites Based on Natural Fibre Fabrics. In: Dubrovski PD, editor. Woven Fabr. Eng., IntechOpen; 2010. doi:10.5772/10465.

[5] Sharaf T, Shawkat W, Fam A. Structural performance of sandwich wall panels with different foam core densities in one-way bending. J Compos Mater 2010;44:2249–63. doi:10.1177/0021998310369577.

[6] Gupta N, Woldesenbet E, Kishore, Sankaran S. Response of Syntactic Foam Core Sandwich Structured Composites to Three-Point Bending. J Sandw Struct Mater 2002;4:249–72. doi:10.1106/109963602024140.

[7] Petras A, Sutcliffe MPF. Failure mode maps for honeycomb sandwich panels. Compos Struct 1999;44:237–52. doi:10.1016/S0263-8223(98)00123-8.

[8] Manalo A, Surendar S, van Erp G, Benmokrane B. Flexural behavior of an FRP sandwich system with glass-fiber skins and a phenolic core at elevated in-service temperature. Compos Struct 2016;152:96–105. doi:10.1016/j.compstruct.2016.05.028.

[9] Besant T, Davies GAO, Hitchings D. Finite element modelling of low velocity impact of composite sandwich panels. Compos - Part A Appl Sci Manuf 2001;32:1189–96. doi:10.1016/S1359-835X(01)00084-7.

[10] Manalo AC, Aravinthan T, Karunasena W, Islam MM. Flexural behaviour of structural fibre composite sandwich beams in flatwise and edgewise positions. Compos Struct 2010;92:984–95. doi:10.1016/j.compstruct.2009.09.046.

[11] Dai J, Hahn HT. Flexural behavior of sandwich beams fabricated by vacuum-assisted resin transfer molding. Compos Struct 2003;61:247–53. doi:10.1016/S0263-8223(03)00040-0.

[12] Fam A, Sharaf T. Flexural performance of sandwich panels comprising polyurethane core and GFRP skins and ribs of various configurations. Compos Struct 2010;92:2927–35. doi:10.1016/j.compstruct.2010.05.004.

[13] Betts D, Sadeghian P, Fam A. Experimental Behavior and Design-Oriented Analysis of Sandwich Beams with Bio-Based Composite Facings and Foam Cores. J Compos Constr 2018;22:1–12.

[14] Mak K, Fam A, Macdougall C. Flexural Behavior of Sandwich Panels with Bio-FRP Skins Made of Flax Fibers and Epoxidized Pine-Oil Resin. J Compos Constr 2015;19:1–13. doi:10.1061/(ASCE)CC.1943-5614.0000560.

[15] Mak K, Fam A. Performance of flax-FRP sandwich panels exposed to different ambient temperatures. Constr Build Mater 2019;219:121–30. doi:10.1016/j.conbuildmat.2019.05.118.

[16] Codyre L, Mak K, Fam A. Flexural and axial behaviour of sandwich panels with bio-based flax fibre-reinforced polymer skins and various foam core densities. J Sandw Struct Mater 2016:1–22. doi:10.1177/1099636216667658.

[17] Abrate S. Localized Impact on Sandwich Structures With Laminated Facings. Appl Mech Rev 1997;50:69. doi:10.1115/1.3101689.

[18] Anderson T, Madenci E. Experimental investigation of low-velocity impact characteristics of sandwich composites. Compos Struct 2000;50:239–47. doi:10.1016/S0263-8223(00)00098-2.

[19] Atas C, Potoglu U. The Effect of Face-Sheet Thickness on Low-Velocity Impact Response of Sandwich Composites with Foam Cores. J Sandw Struct Mater 2016;18:215–28. doi:10.1177/1099636215613775.

[20] Schubel PM, Luo J-J, Daniel IM. Low velocity impact behavior of composite sandwich panels. Compos Part A Appl Sci Manuf 2005;36:1389–96. doi:10.1016/j.compositesa.2004.11.014.

[21] Torre L, Kenny JM. Impact testing and simulation of composite sandwich structures for civil transportation. Compos Struct 2000;50:257–67. doi:10.1016/S0263-8223(00)00101-X.

[22] Akil Hazizan M, Cantwell WJ. The low velocity impact response of foam-based sandwich structures. Compos Part B Eng 2002;33:193–204. doi:10.1016/S1359-8368(02)00009-4.

[23] Plagianakos TS, Lika K, Papadopoulos EG. Low-velocity impact response of smart sandwich composite plates with piezoelectric transducers : Modeling and experiments. J Intell Mater Syst Struct 2016;27:774–85. doi:10.1177/1045389X15580662.

[24] Boria S, Raponi E, Sarasini F, Tirillò J, Lampani L. Green sandwich structures under impact: experimental vs numerical analysis. Procedia Struct Integr 2018;12:317–29. doi:10.1016/j.prostr.2018.11.084.

[25] Ude AU, Arif AK, Azhari CH. Impact damage characteristics in reinforced woven natural silk / epoxy composite face-sheet and sandwich foam, coremat and honeycomb materials. Int J Impact Eng 2013;58:31–8. doi:10.1016/j.ijimpeng.2013.03.003.

[26] Betts D, Sadeghian P, Fam A. Experiments and nonlinear analysis of the impact behaviour of sandwich panels constructed with flax fibre-reinforced polymer faces and foam cores. J Sandw Struct Mater 2020. doi:10.1177/1099636220925073.

[27] Hu J, Yin S, Yu TX, Xu J. Dynamic compressive behavior of woven flax-epoxy-laminated composites. Int J Impact Eng 2018;117:63–74. doi:10.1016/j.ijimpeng.2018.03.004.

[28] Kim W, Argento A, Lee E, Flanigan C, Houston D, Harris A, et al. High strain-rate behavior of natural fiber-reinforced polymer composites. J Compos Mater 2012;46:1051–65. doi:10.1177/0021998311414946.

[29] Shipsha A, Zenkert D. Compression-after-impact strength of sandwich panels with core crushing damage. Appl Compos Mater 2005;12:149–64. doi:10.1007/s10443-005-1119-1.

[30] Gustin J, Joneson A, Mahinfalah M, Stone J. Low velocity impact of combination Kevlar/carbon fiber sandwich composites. Compos Struct 2005;69:396–406. doi:10.1016/j.compstruct.2004.07.020.

[31] Davies GAO, Hitchings D, Besant T, Clarke A, Morgan C. Compression after impact strength of composite sandwich panels. Compos Struct 2004;63:1–9. doi:10.1016/S0263-8223(03)00119-3.

[32] Baran I, Weijermars W. Residual bending behaviour of sandwich composites after impact. J Sandw Struct Mater 2020;22:402–22. doi:10.1177/1099636218757164.

[33] He W, Liu J, Wang S, Xie D. Low-velocity impact response and post-impact flexural behaviour of composite sandwich structures with corrugated cores. Compos Struct 2018;189:37–53. doi:10.1016/j.compstruct.2018.01.024.

[34] Klaus M, Reimerdes HG, Gupta NK. Experimental and numerical investigations of residual strength after impact of sandwich panels. Int J Impact Eng 2012;44:50–8. doi:10.1016/j.ijimpeng.2012.01.001.

[35] Göttner W, Reimerdes HG. Bending strength of sandwich panels with different cores after impact. Fract. Nano Eng. Mater. Struct. - Proc. 16th Eur. Conf. Fract., 2006, p. 1261–2. doi:10.1007/1-4020-4972-2_626.

[36] Betts D, Sadeghian P, Fam A. Experiments and Nonlinear Analysis of the Impact Behavior of Sandwich Panels Constructed with Flax Fibre-Reinforced Polymer Faces and Foam Cores. J Sandw Struct Mater n.d.

[37] Christian SJ, Billington SL. Mechanical response of PHB- and cellulose acetate natural fiber-

reinforced composites for construction applications. Compos Part B 2011;42:1920–8. doi:10.1016/j.compositesb.2011.05.039.

[38] Yan L, Kasal B, Huang L. A review of recent research on the use of cellulosic fibres, their fibre fabric reinforced cementitious, geo-polymer and polymer composites in civil engineering. Compos Part B Eng 2016;92:94–132. doi:10.1016/j.compositesb.2016.02.002.

[39] Mathura N, Cree D. Characterization and mechanical property of Trinidad coir fibers. J Appl Polym Sci 2016;133:1–9. doi:10.1002/app.43692.

[40] Hristozov D, Wroblewski L, Sadeghian P. Long-term tensile properties of natural fibre-reinforced polymer composites: Comparison of flax and glass fibres. Compos Part B Eng 2016;95:82–95. doi:10.1016/j.compositesb.2016.03.079.

[41] ASTM. ASTM D7136, Standard test method for measuring the damage resistance of a fiber-reinforced polymer matrix composite to a drop-weight impact event. Annu B ASTM Stand 2005:1–16. doi:10.1520/D7136.

[42] ASTM. D790, Standard Test Methods for Flexural Properties of Unreinforced and Reinforced Plastics and Electrical Insulating Materials. Annu B ASTM Stand 2017:12. doi:10.1520/D0790-17.2.

Table 1: Test matrix

Specimen	Test Group	Core Density, kg/m^3	FFRP Layers	Width, mm	Impact Energy, J	No. of Impacts
1FL-C32-R100	R100	32	1	151.1	10.2	1
2FL-C32-R100	R100	32	2	149.5	30.6	1
3FL-C32-R100	R100	32	3	150.6	91.9	1
1FL-C64-R100	R100	64	1	151.0	30.6	1
2FL-C64-R100	R100	64	2	151.6	122.6	1
3FL-C64-R100	R100	64	3	151.9	173.7	1
1FL-C96-R100	R100	96	1	152.1	61.3	1
2FL-C96-R100	R100	96	2	151.9	163.4	1 †
3FL-C96-R100	R100	96	3	152.1	245.1	1
1FL-C32-R75	R75	32	1	76.0	9.8 *	6 †
2FL-C32-R75	R75	32	2	77.4	23.5 *	5 †
3FL-C32-R75	R75	32	3	79.6	48.7	3 †
1FL-C64-R75	R75	64	1	74.5	15.3	50
2FL-C64-R75	R75	64	2	74.3	27.1	50
3FL-C64-R75	R75	64	3	76.4	34.5	50
1FL-C96-R75	R75	96	1	75.7	23.7	14 †
2FL-C96-R75	R75	96	2	74.2	68.5	6 †
3FL-C96-R75	R75	96	3	72.9	100.0	24 †
1FL-C32-R50	R50	32	1	74.6	5.3	50
2FL-C32-R50	R50	32	2	72.0	11.7	50
3FL-C32-R50	R50	32	3	20.3	27.7	24 †
1FL-C64-R50	R50	64	1	75.7	10.3	50
2FL-C64-R50	R50	64	2	69.7	16.9	50
3FL-C64-R50	R50	64	3	75.0	22.6	50
1FL-C96-R50	R50	96	1	75.5	15.8	50
2FL-C96-R50	R50	96	2	77.1	47.5	50
3FL-C96-R50	R50	96	3	78.6	71.9	50

* *These specimens were tested at 90% of energy resisted by static specimens*

† *Specimen failed during impact tests*

Table 2: Load capacity of post-impact flexural tests

Specimen Type	Static Load Capacity (S), kN *	Static Failure Mode	Residual Load Capacity After 50 Impacts at 50% Energy (R50), kN	R50/S Ratio	R50 Failure Mode	Residual Load Capacity After 50 Impacts at 75% Energy (R75), kN	R75/S Ratio	R75 Failure Mode	Residual Load Capacity After One Impact at 100% Energy (R100), kN	R100/S Ratio	R100 Failure Mode
1FL-C32	0.65	CC/CW	0.47	0.71	CW	-	-	-	0.65	1.00	CW
2FL-C32	1.17	CS	1.27	1.08	CS	-	-	-	1.28	1.09	CS
3FL-C32	1.53	CS	-	-	-	-	-	-	1.72	1.12	CS
1FL-C64	1.18	CC/CW	1.37	1.16	CC	1.41	1.19	TR/CC	1.23	1.04	CW
2FL-C64	1.63	CW	2.32	1.42	CS	1.84	1.13	CC	2.07	1.27	CC
3FL-C64	2.31	CS	2.77	1.20	CS	2.64	1.14	CS/CC	2.73	1.18	CS
1FL-C96	1.54	TR	1.46	0.95	TR	-	-	-	1.76	1.14	TR
2FL-C96	3.35	TR	2.96	0.88	TR	-	-	-	-	-	-
3FL-C96	4.54	TR/CS	4.86	1.07	TR	-	-	-	4.80	1.06	TR
AVE				1.06			1.16			1.11	
SD				0.20			0.03			0.08	

All data was normalised to a beam width of 75 mm

AVE = Average, SD = Standard Deviation, CC = Compression Crushing, CW = Compression Wrinkling, CS = Core Shear, TR = Tensile Rupture

** Data from Betts et al (2018)*

Table 3: Stiffness of post-impact flexural test specimens

Specimen Type	Static Stiffness (S), kN/m *	Stiffness After 50 Impacts at 50% Energy (R50), kN/m	R50/S Ratio	Stiffness After 50 Impacts at 75% Energy (R75), kN/m	R75/S Ratio	Stiffness After One Impact at 100% Energy (R100), kN/m	R100/S Ratio
1FL-C32	26.77	23.77	0.89	-	-	30.26	1.13
2FL-C32	38.43	38.35	1.00	-	-	34.32 †	0.89
3FL-C32	43.38	-	-	-	-	44.06	1.02
1FL-C64	52.84	44.01	0.83	45.80	0.87	47.88	0.91
2FL-C64	58.13	62.71	1.08	66.41	1.14	69.83	1.20
3FL-C64	80.63	79.59	0.99	76.81	0.95	86.46	1.07
1FL-C96	61.36	57.58	0.94	-	-	59.26	0.97
2FL-C96	101.55	91.79	0.90	-	-	-	-
3FL-C96	124.31	120.62	0.97	-	-	116.89	0.94
AVE			0.95		0.99		1.02
SD			0.07		0.12		0.10

1. *All data was normalised to a beam width of 75 mm*
2. *Stiffnesses were determined by fitting a line to the data between load-deflection data between deflections of 1 mm and 5 mm.*

* *Data from Betts et al (2018)*

† *Stiffness was determined between deflections of 5 mm and 7 mm due to a lack of data below 5 mm.*

LIST OF FIGURES

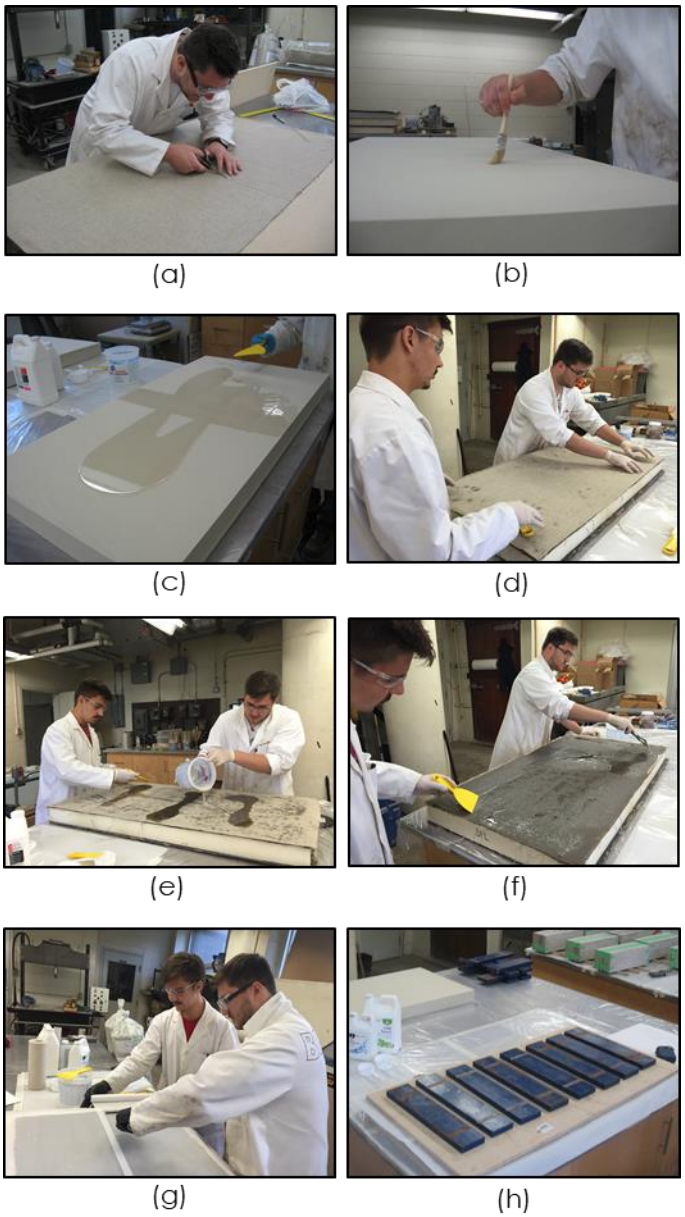

Figure 1. Specimen fabrication: (a) cutting fabric; (b) cleaning foam surface; (c) applying epoxy resin to foam surface; (d) placement of flax fabric; (e) placing epoxy resin flax fabric; (f) spreading epoxy resin over surface of flax fabric; (g) removal of air and excess resin; and (h) curing with weighted board

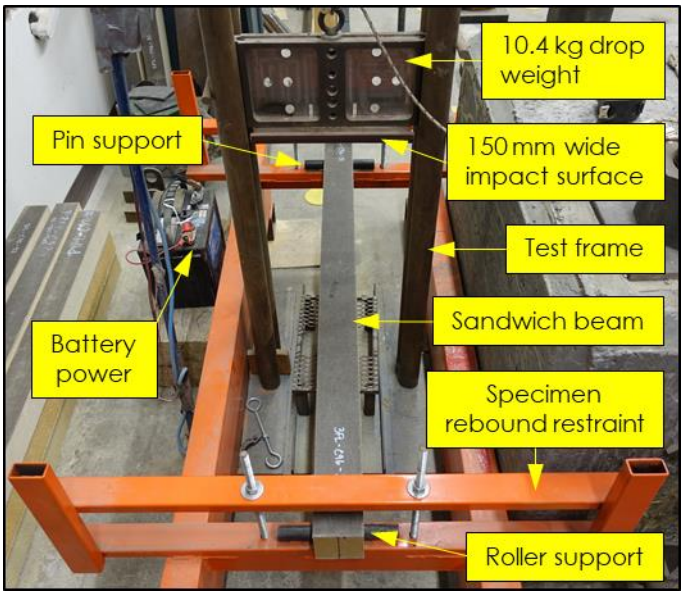

Figure 2. Impact test set-up

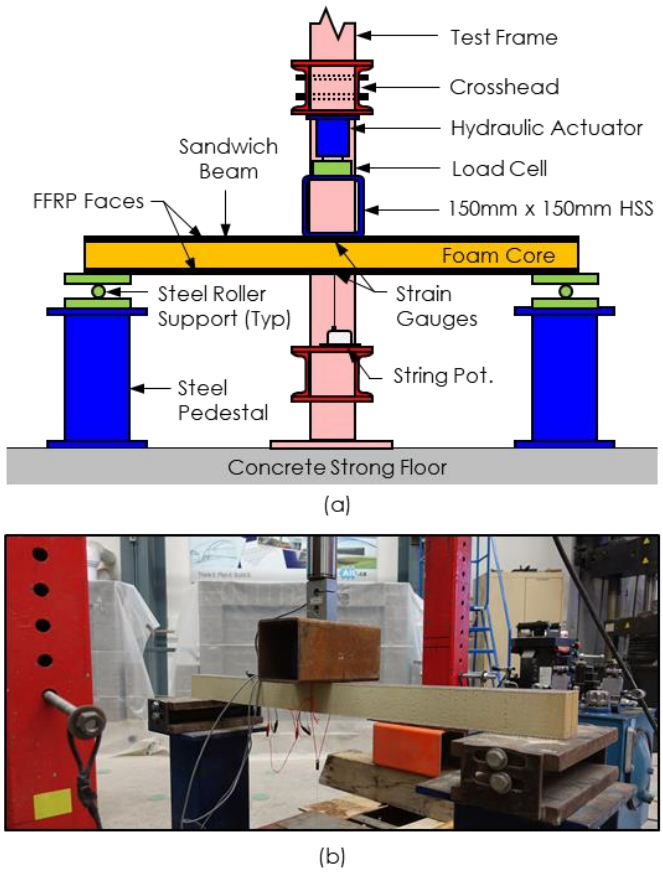

Figure 3. Residual bending test set-up (a) schematic and; (b) photo (R50 specimen)

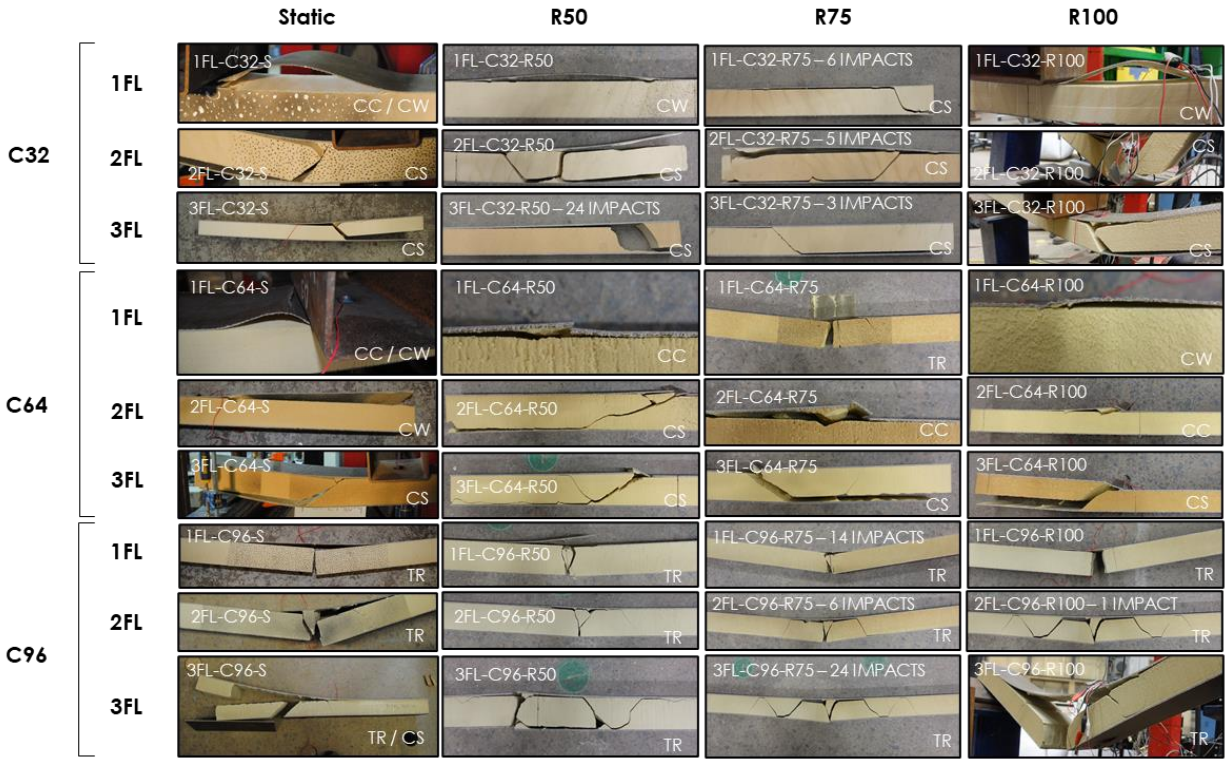

Figure 4. Failure modes of all specimens [Note static specimens were tested as a part of another study by Betts et al (2018)]

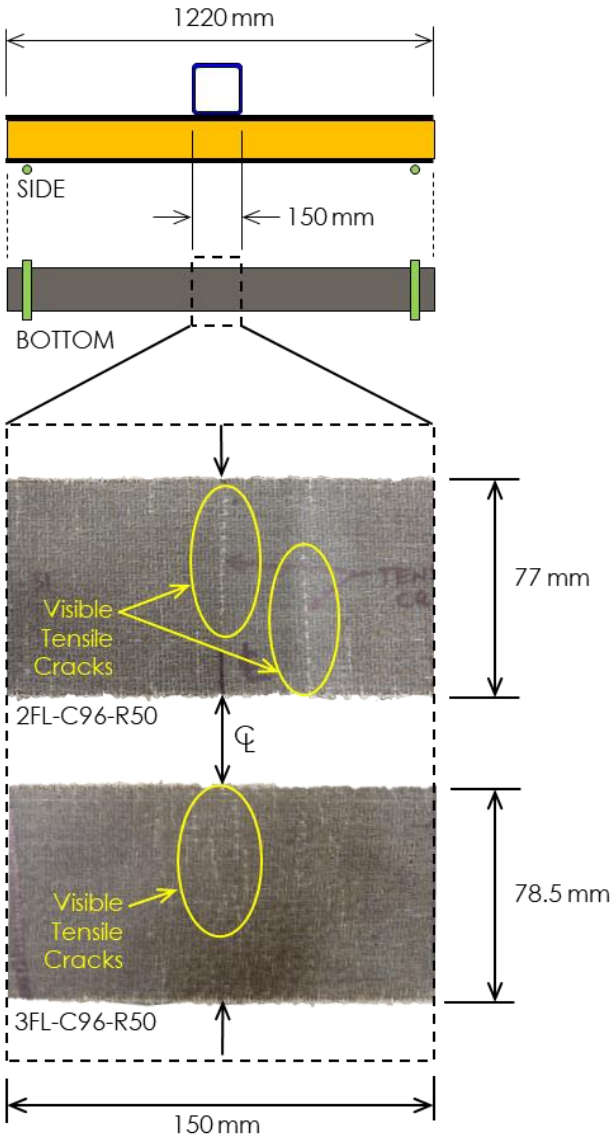

Figure 5. Tensile cracking evident on bottom face of impacted specimens 2FL-C96-R50 and 3FL-C96-R50

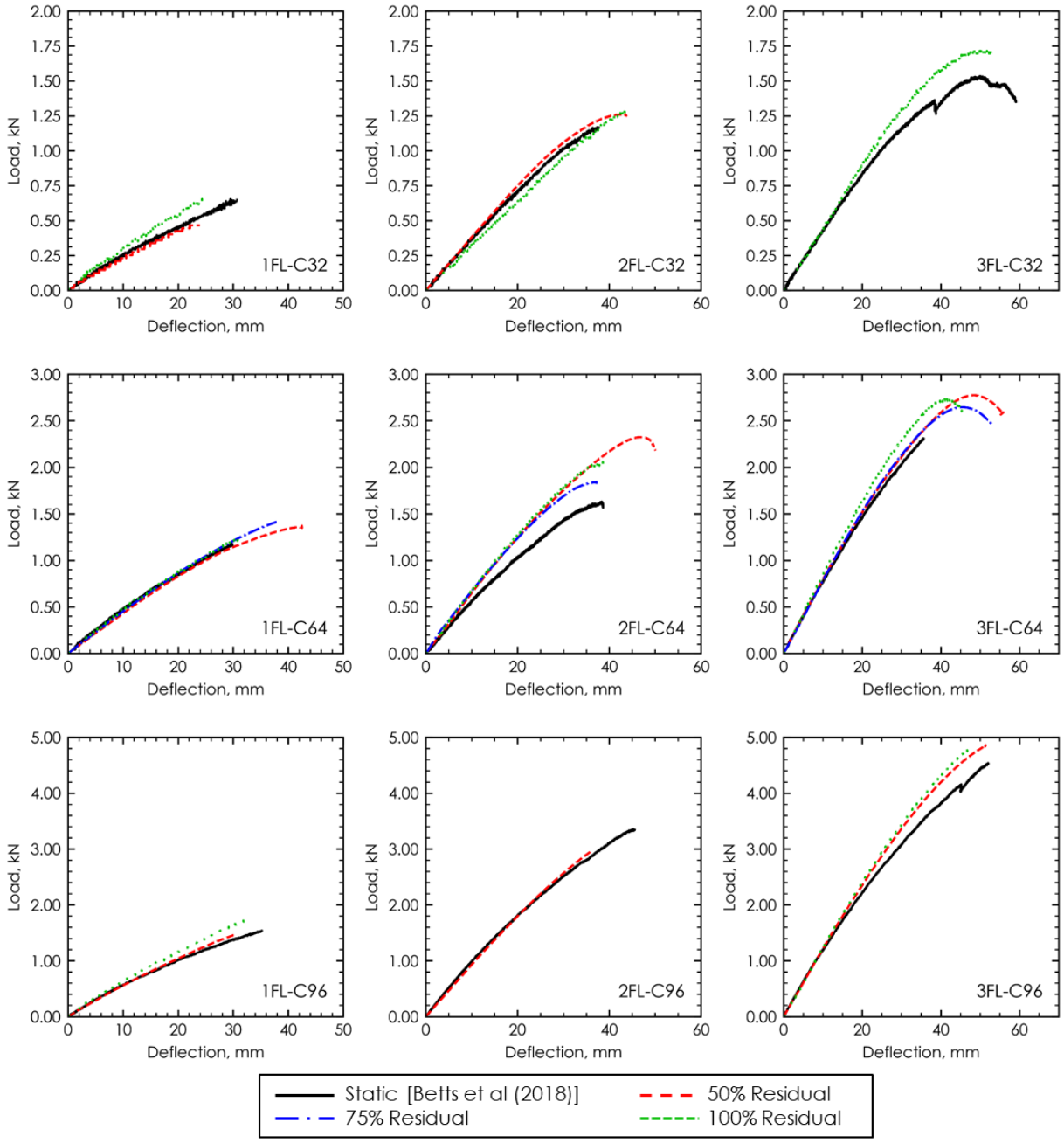

Figure 6. Residual load-deflection diagrams (normalised to a beam width of 75 mm)

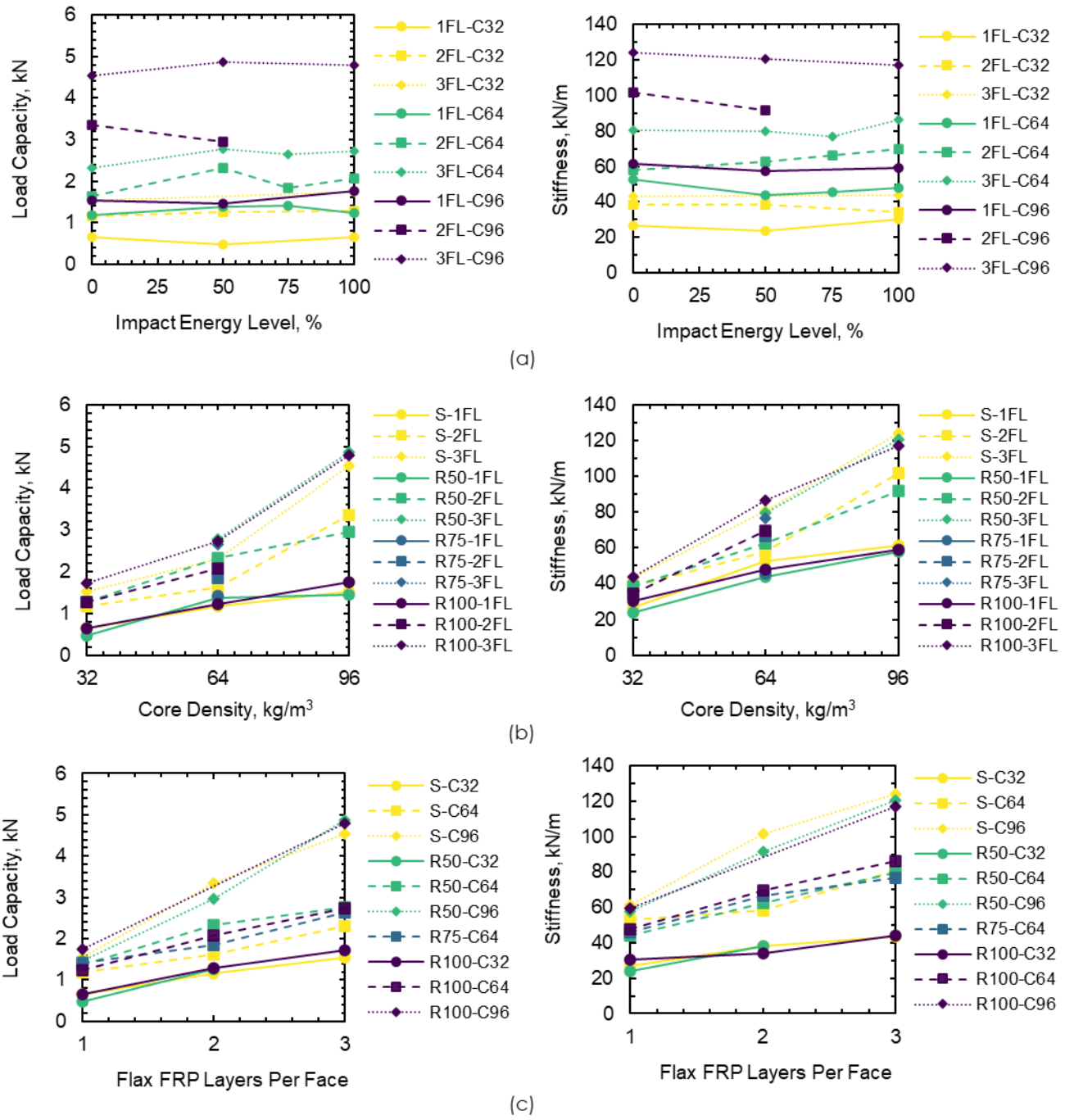

Figure 7. Post-impact load capacity and stiffness – effect of (a) impact energy level; (b) core density; and (c) flax FRP layers per face

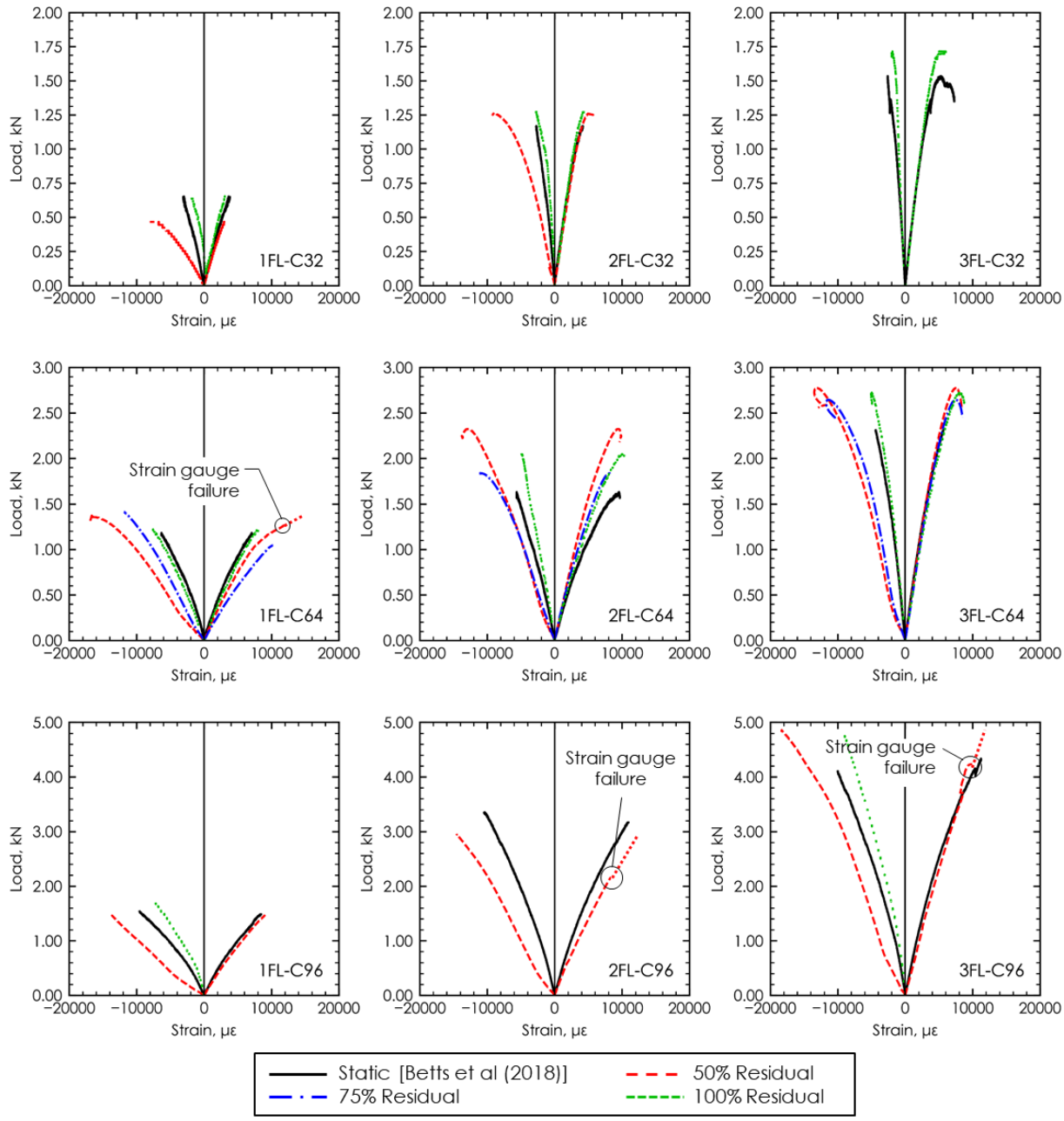

Figure 8. Residual load-strain diagrams with compressive strain shown as negative and tensile strain shown as positive (normalised to a beam width of 75 mm)

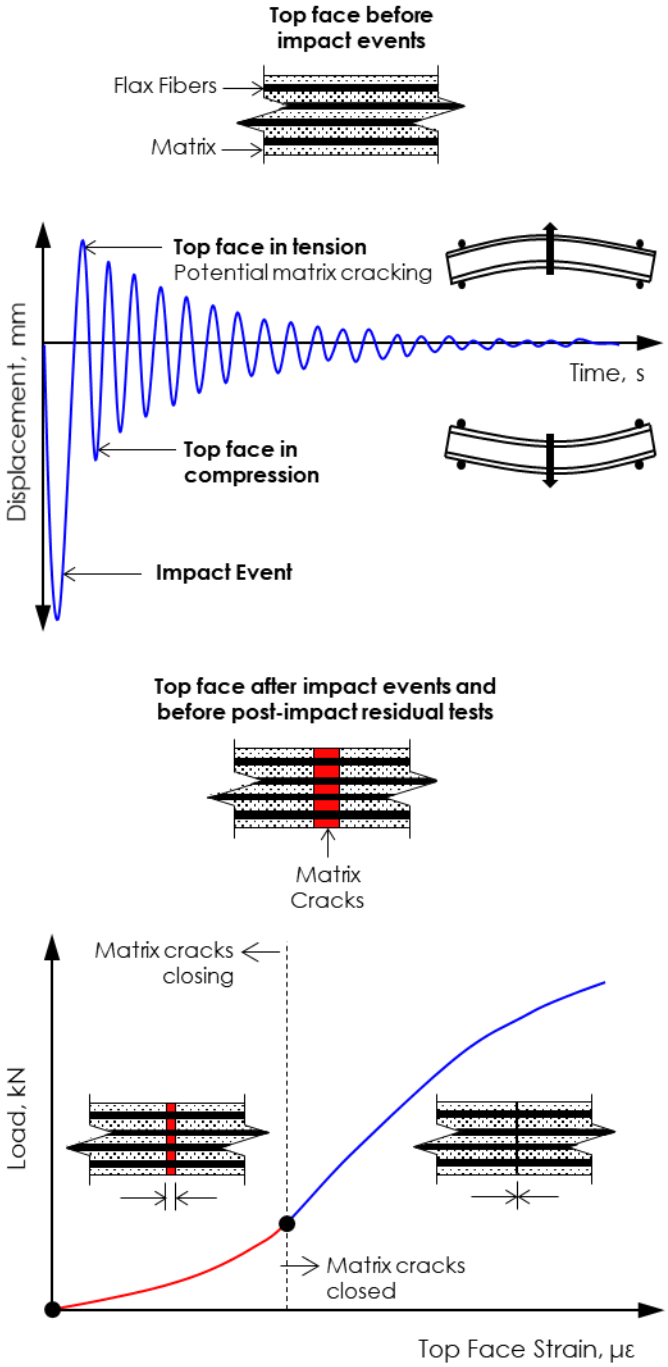

Figure 9. Hypothesis for the cause of increasing stiffness on compression face of impacted sandwich beams

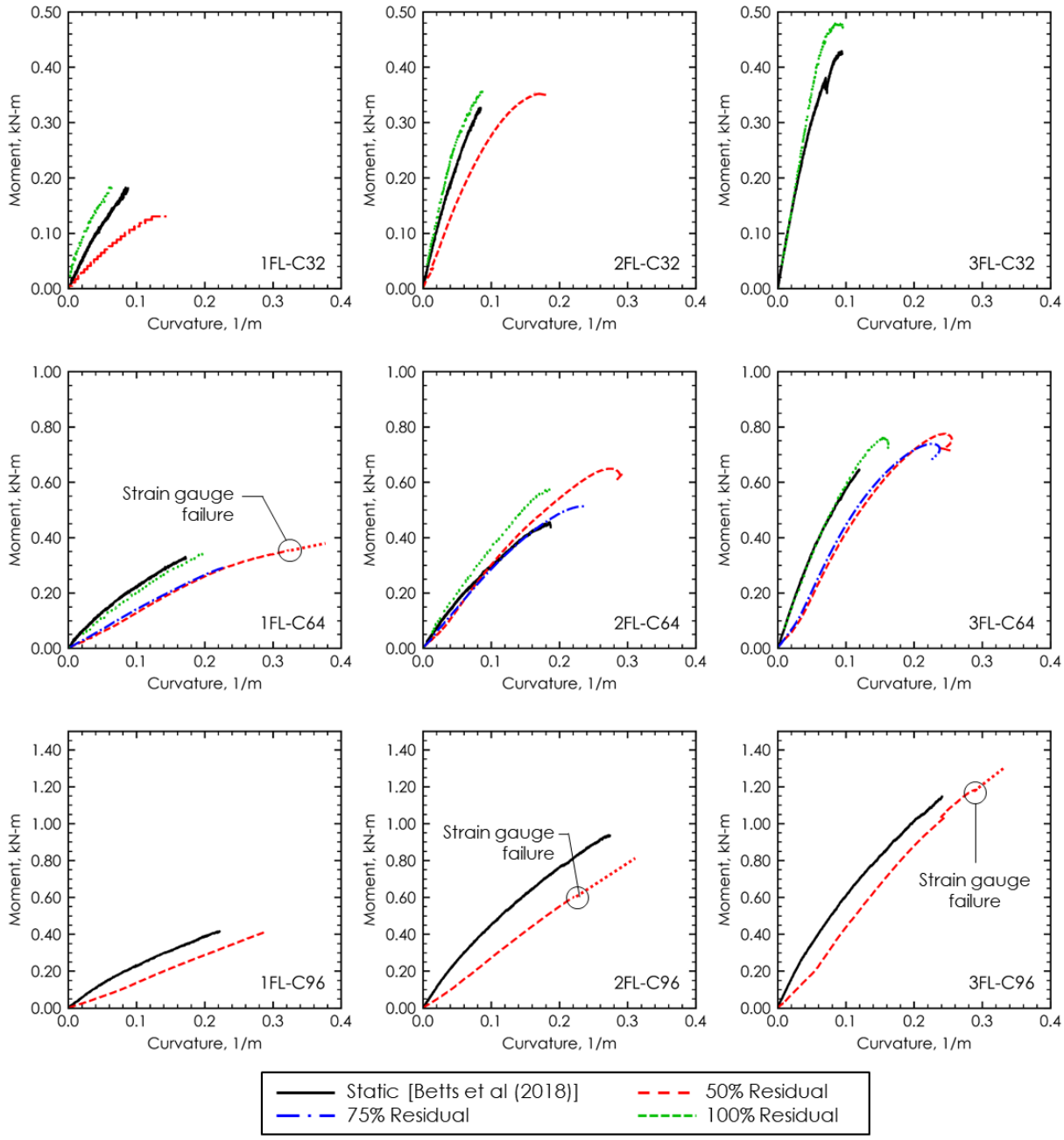

Figure 10. Residual moment-curvature diagrams (normalised to a beam width of 75 mm)